Journal of Advanced Ceramics
2023, **12**(5): 1105–1117
https://doi.org/10.26599/JAC.2023.9220730
ISSN 2226-4108
CN 10-1154/TQ

Research Article

Ultrasound-driven $BaTiO_3$ nanorobots patching immunologic barrier to cure chronic rheumatoid arthritis

Le Jiang[a,b,†], Yifan Wang[a,b,†], Chunlin Liu[a,b,†], Nan Xu[a,b], Wenshuo Li[a,b], Lei Wang[c], Yixian Wu[a,b], Jingyun Wang[a,b], Zhijun He[a,b], Fengbo Sun[a,b], Lingyun Zhao[a,b], Qiong Wu[c], Xiumei Wang[a,b], Huihui Yuan[d,*], Xiaohui Wang[a,b,*], Xiaodan Sun[a,b,*]

[a]*State Key Laboratory of New Ceramics and Fine Processing*, *School of Materials Science and Engineering*, *Tsinghua University*, *Beijing 100084*, *China*
[b]*Key Laboratory of Advanced Materials of Ministry of Education of China*, *School of Materials Science and Engineering*, *Tsinghua University*, *Beijing 100084*, *China*
[c]*MOE Key Lab. Bioinformatics*, *School of Life Sciences*, *Tsinghua University*, *Beijing 100084*, *China*
[d]*Department of Immunology*, *School of Basic Medical Sciences*, *Capital Medical University*, *Beijing 100069*, *China*

Received: December 3, 2022; Revised: January 1, 2023; Accepted: February 4, 2023

Abstract: The disruption and reconstruction of the $TREM2^+$ tissue resident macrophage (TRM) barrier on the surface of synovial lining play a key role in the activation and "remission" of rheumatoid arthritis (RA), which engender the prediction of this immunologic barrier as a potential driver for the achievement of "cure" in RA. However, strategies to promote the reconstruction of this barrier have not been reported, and the effect of patching this barrier remains unidentified. On the other hand, appropriate piezoelectric stimulation can reprogram macrophages, which has never been exerted on this barrier TRM yet. Herein, we design piezoelectric tetragonal $BaTiO_3$ (BTO) ultrasound-driven nanorobots (USNRs) by the solvothermal synthesis method, which demonstrates satisfactory electro-mechanical conversion effects, paving the way to generate controllable electrical stimulation under ultrasound to reprogram the barrier TRM by minimally invasive injection into joint cavity. It is demonstrated that the immunologic barrier could be patched by this USNR effectively, thereby eliminating the hyperplasia of vessels and nerves (HVN) and synovitis. Additionally, TREM2 deficiency serum-transfected arthritis (STA) mice models are applied and proved the indispensable role of TREM2 in RA curing mediated by USNR. In all, our work is an interesting and important exploration to expand the classical tetragonal BTO nanoparticles in the treatment of autoimmune diseases, providing a new idea and direction for the biomedical application of piezoelectric ceramics.

Keywords: ultrasound-driven; $BaTiO_3$ nanorobots (BTO NRs); immunologic barrier; upstream driver; rheumatoid arthritis (RA)

† Le Jiang, Yifan Wang, and Chunlin Liu contributed equally to this work.

* Corresponding authors.
E-mail: H. Yuan, huihuiyuan@mail.ccmu.edu.cn;
X. Wang, wxh@mail.tsinghua.edu.cn;
X. Sun, sunxiaodan@tsinghua.edu.cn

1 Introduction

Rheumatoid arthritis (RA), a common autoimmune disease, is characterized by chronic synovitis and synovial tissue structural changes, including hyperplasia of vessels and nerves (HVN) [1]. In this disease, synovial cells, dominated by macrophages and synovial fibroblasts, form invasive pannus together with high density blood vessels and nerves, which will gradually erode the osteocartilage, causing severe pain and eventually disability [2–4]. In the past 20 years, treat to target (T2T) has become the most recommended general principle of RA treatment, and the primary goal of T2T is to relieve disease symptoms. Recently, Schett *et al*. [2] pointed out that the therapy effect of T2T can only be defined as "remission", where the alleviation of synovitis was achieved by blockade of specific effector cytokines and their respective downstream pathways. At the same time, it is emphasized that curing RA by paying attention to the potential drivers would become the goal of next-generation therapy. Therefore, exploring new strategies based on the potential drivers of curing RA poses new challenges for the clinical and scientific research of RA.

In 2019, Culemann *et al*. [5] discovered a $TREM2^+$ tissue resident macrophage (TRM) barrier on the surface of synovial lining, which has been reported to play a key role in the development and remission of RA [6]. Usually, this immunologic barrier physically prevents pro-inflammatory factors and blood-derived inflammatory cells from entering the joint cavity [5]. Once RA occurs, the morphology and spatial orientation of $TREM2^+$ TRM will change rapidly, causing the disruption of the immunologic barrier. Meanwhile, it was reported that the barrier could be restored when RA was in remission [6]. Therefore, patching this immunologic barrier is expected to be the potential driver to cure RA [2]. However, strategies to promote the reconstruction of this barrier has not been reported, and the effect of patching this barrier remains unidentified. Dai *et al*. [7] discovered that the polarized $BaTiO_3$/poly(vinylidene fluoride–trifluoroethylene) (BTO/P(VDF–TrFE)) nanocomposite membranes can switch macrophage phenotype from the pro-inflammatory (M1) into the pro-healing (M2) phenotype, which demonstrated that appropriate piezoelectric stimulation can reprogram macrophages including inducing anti-inflammatory phenotype, which may help to patch this barrier [7–11].

BTO is suitable for piezoelectric biomaterials because Refs. [12,13] have shown that it has no cytotoxic effect. Herein, we prepare BTO nanoparticles by the solvothermal synthesis method, which are characterized as uniformly distributed size, tetragonal phase, and nearly defect-free single crystal. The BTO nanoparticles performed satisfactory electro-mechanical response, as shown in the typical butterfly amplitude curve and a 180° phase switching in the standard square hysteresis loop. Furthermore, the nanoparticles are calculated to be able to generate a 35 mV surface potential under an ultrasound (US) of 1 W/cm^2. Therefore, we define such nanoparticles as ultrasound-driven nanorobots (USNRs), which can generate controllable electrical stimulation in response to ultrasound to cure RA by minimally invasive injection into joint cavity with the collagen carrier. It was demonstrated that the immunologic barrier could be patched by USNR effectively, thereby eliminating RA symptoms and pathologies, including HVN and synovitis.

Additionally, TREM2 has been reported to play an important role in other pathological processes such as Alzheimer's disease, where inhibiting hydrolysis and abscission of TREM2 can promote macrophage phagocytosis, increase macrophage survival, and inhibit inflammation [14–21]. However, the role of TREM2 in RA has not been reported so far. More importantly, it has been reported that TREM2 prefers to bind with negatively charged ligand [15]. Therefore, in order to further explore the potential molecular mechanism of USNR for RA treatment, we are inspired to study the behaviors of $TREM2^+$ TRM, which may be influenced by the change of the intrinsic binding between TREM2 with negatively charged ligand via the charges generated by USNR. It is demonstrated in this work that the BTO USNR promotes the repair of the macrophage barrier by reconnecting $TREM2^+$ TRM (Fig. 1). Furthermore, to validate the role of TREM2 in the pathogenesis of RA, we use mice with TREM2 knockout, which shows that TREM2 deficiency increases RA symptoms and pathology in serum-transfected arthritis (STA) mouse models. And USNR does not effectively relieve inflammation in TREM2 knockout STA mice compared with normal STA mice. In conclusion, the potential mechanism of USNR in treating RA is mediated by TREM2 molecules.

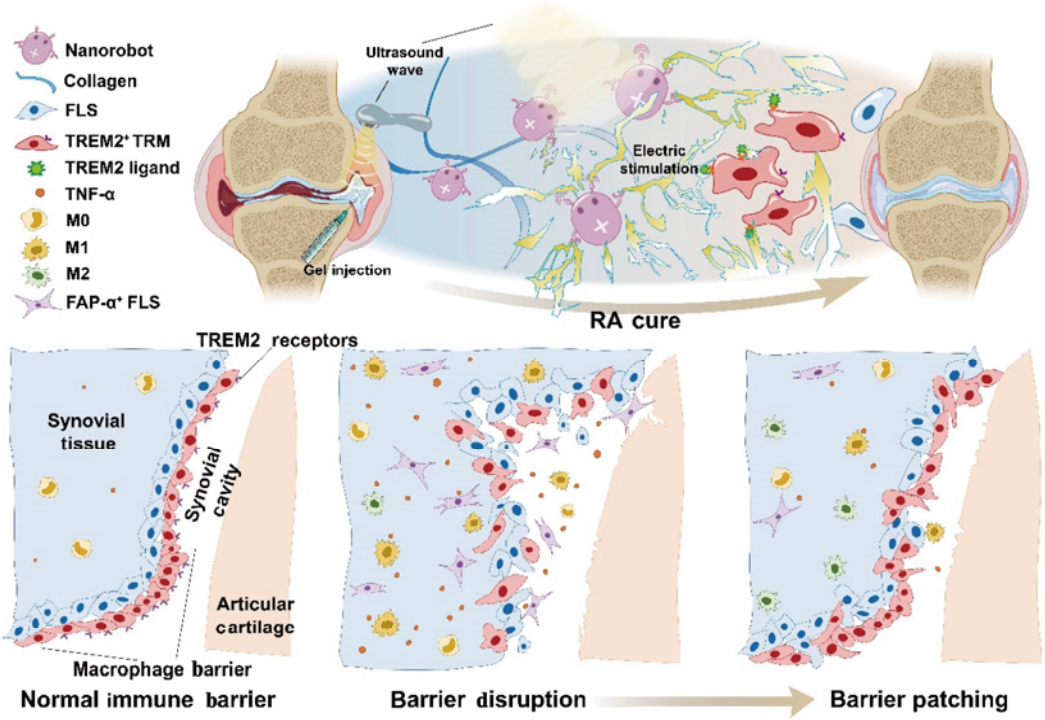

Fig. 1 Schematic illustration of USNR patching immunologic barrier to cure chronic RA.

In all, our work is an interesting and important exploration to expand the classical tetragonal BTO nanoparticles in the treatment of autoimmune diseases, providing a new idea and direction for the biomedical application of piezoelectric ceramics.

2 Characterization of NR

BTO nanoparticles, which are selected to act as piezoelectric NRs due to their outstanding smart ability to release electrical signals responding to mechanical energy, are synthesized by the solvothermal method. They are mostly obtuse-angle cuboid with a uniform diameter (average value ≈ 82.58 nm) (Figs. 2(a), 2(b), 2(e), and 2(i)), while the hydrated average particle size is 322.8 nm (Fig. S3 in the Electronic Supplementary Material (ESM)). The elemental mapping results (Figs. 2(f)–2(h)) show that the NR contains a large number of evenly distributed O, Ba, and Ti, which preliminarily confirms the composition of the synthetic product. In the characterization of the X-ray photoelectron spectroscopy (XPS), the compositions of Ba, Ti, and O are also confirmed by full spectrum scanning (Fig. S4 in the ESM). For the narrow scans, the peaks at 795.25 and 780.05 eV correspond to Ba $3d_{3/2}$ and Ba $3d_{5/2}$, respectively (Fig. 2(k)), while the peaks at 458.80, 464.65, 529.80, and 532.45 eV correspond to Ti $2p_{3/2}$, Ti $2p_{1/2}$, O 1s, and adsorbed oxygen, respectively (Fig. S4 in the ESM), which are consistent with the reported XPS spectrum of BTO. The piezoelectricity of BTO originates from the deviation of Ti ions from the B-site of the standard perovskite structure (ABO_3) with a tetragonal phase, which produces a dipole moment and also leads to the extension of crystal cells along the *c*-axis of the cube. Therefore, the phase of the synthetic product can be determined through the microscopic quantification of lattice parameters. The lattice constants (a = 0.400778 nm and c = 0.403232 nm) are calculated from the Rietveld refined spectrum (Fig. 2(l)) of the X-ray diffraction (XRD), which shows that the synthesized NRs are in good agreement with the BTO structure with *P*4*mm* space group (JCPDS No. 96-151-3253), and the *c*/*a* value is consistent with the reported value [22].

In addition, the XRD pattern has obvious (002) and (200) splitting peaks at 45°, and the peak strength ratio is approximately 1 : 2, further indicating that the NR obtained here had a good tetragonal phase structure. Performing the fast Fourier transform on the lattice patterns in the HRTEM micrograph (Fig. 2(c)), the (001) and (100) planes with crystal plane spacings of 0.411 and 0.406 nm, respectively, were identified, which were similar to the calculated values in the XRD.

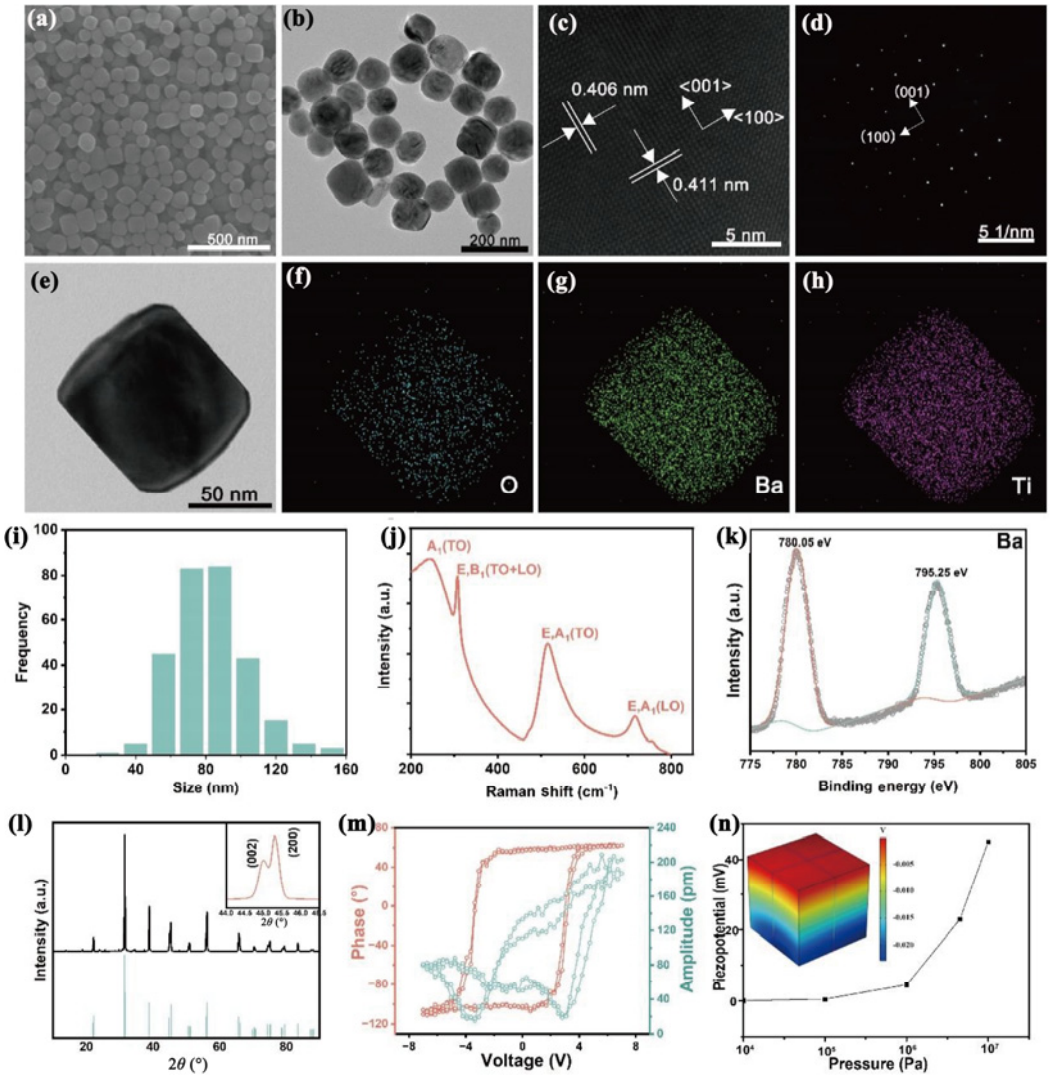

Fig. 2 Characterization of NR. (a) Scanning electron microscopy (SEM) image of NR. (b) Transmission electron microscopy (TEM) image of NR. (c) High-resolution transmission electron microscopy (HRTEM) image of NR. (d) Selected area electron diffraction (SAED) pattern of NR. (e–h) Scanning transmission electron microscopy (STEM) image and corresponding elemental mapping images. (i) Particle size distribution by SEM image of NR. (j) Raman spectra of NR. (k) XPS spectra (Ba) of NR. (l) XRD pattern of T-BTO and enlarged (002) and (200) peaks (the inset). (m) Piezo-responsive phase curve and amplitude curve of NR. (n) Piezopotential distribution in BTO nanocrystals under various cavitation pressures by COMSOL simulation; the inset is the piezopotential distribution nephogram in BTO nanocrystals at a pressure of 4.9×10^5 Pa (equal to an ultrasound ware with power of 1 W/cm^2).

These results are further supported by the SAED pattern (Fig. 2(d)). To further determine the crystal structure, the Raman spectra are analyzed, where the peaks at 246.79, 308.05, 515.67, and 716.77 cm^{-1} correspond to the A1(TO), E,B1(TO+LO), E,A1(TO), and E, A1(LO) types of vibrational scattering, respectively (Fig. 2(j)), which are consistent with the reported tetragonal BTO Raman scattering [22–24]. Since Ti^{4+} in cubic BTO is located in the center of TiO_6 octahedra and has completely symmetrical electrostatic effect, there is no first-order Raman effect in cubic BTO [23,25], so the Raman activity observed here reveals the tetragonal distortion of TiO_6 octahedra. In addition, the clear diagonal lattice stripes of the HRTEM and bright and sharp diffraction spots and the narrow XRD peaks show the single crystal characteristic of NR, and there are no defects such as stacking faults, dislocations, or grain boundaries. To sum up, from the overall analysis of the XRD and the local structure analysis of the TEM and Raman spectra, it is concluded that the solvothermal synthesized NRs exhibit a tetragonal phase structure, which provides an essential structural basis for NRs to exhibit piezoelectricity.

In the piezoresponse force microscopy (PFM) test,

when the bias voltage changed from −7 to 7 V, a butterfly curve was displayed (Fig. 2(m)), indicating mechanical response to varying voltages. At the same time, the phase angle changes 180°, indicating that the ferroelectric domain has achieved 180° reversal after polarization conversion in the coercive field. These results show that the NRs have excellent piezoelectric properties. With the help of COMSOL multiphysics software, the response of a single NR to US is simulated by the finite element method (FEM) (Fig. 2(n) and Figs. S1 and S2 in the ESM). These results show that solvothermal NR can realize the conversion from mechanical energy to electrical energy through US, which provides a basis for the use of NR for US-driven electric generation. For further *in vivo* treatment, NRs are incorporated into injectable collagen hydrogel, which can crosslink under 37 ℃. (Fig. S5 in the ESM) NRs are demonstrated to be evenly dispersed in the hydrogel three-dimensional (3D) network by the SEM characterization (Fig. S6 in the ESM).

3 USNR eliminating RA symptoms and pathologies

In order to evaluate the curing effect of USNR in the treatment of RA, an STA model is obtained by injecting the serum of K/BxN mice. Six groups are set, including normal mouse+saline (NS), STA, Gel, Gel+US, Gel+NR, and Gel+NR+US. After injection of piezoelectric NR hydrogel into the knee joint, US radiation is performed at day 1, day 3, and day 5 (Fig. 3(a)). The US parameters were selected from US1, US2, US3, and US4 (see Section 8 and the ESM for details) by *in vitro* experiments (Figs. 4(i), 4(j), and S7 in the ESM). Compared with STA, Gel, and Gel+US groups, Gel+NR group slightly alleviates RA, while Gel+NR+US significantly inhibits the incidence, reducing clinical scores and joint swelling compared with any other treatment groups (Figs. 3(b)–3(d)). This may be explained that physiological exercise can provide slightly mechanical energy for NR, and the resulting piezoelectric

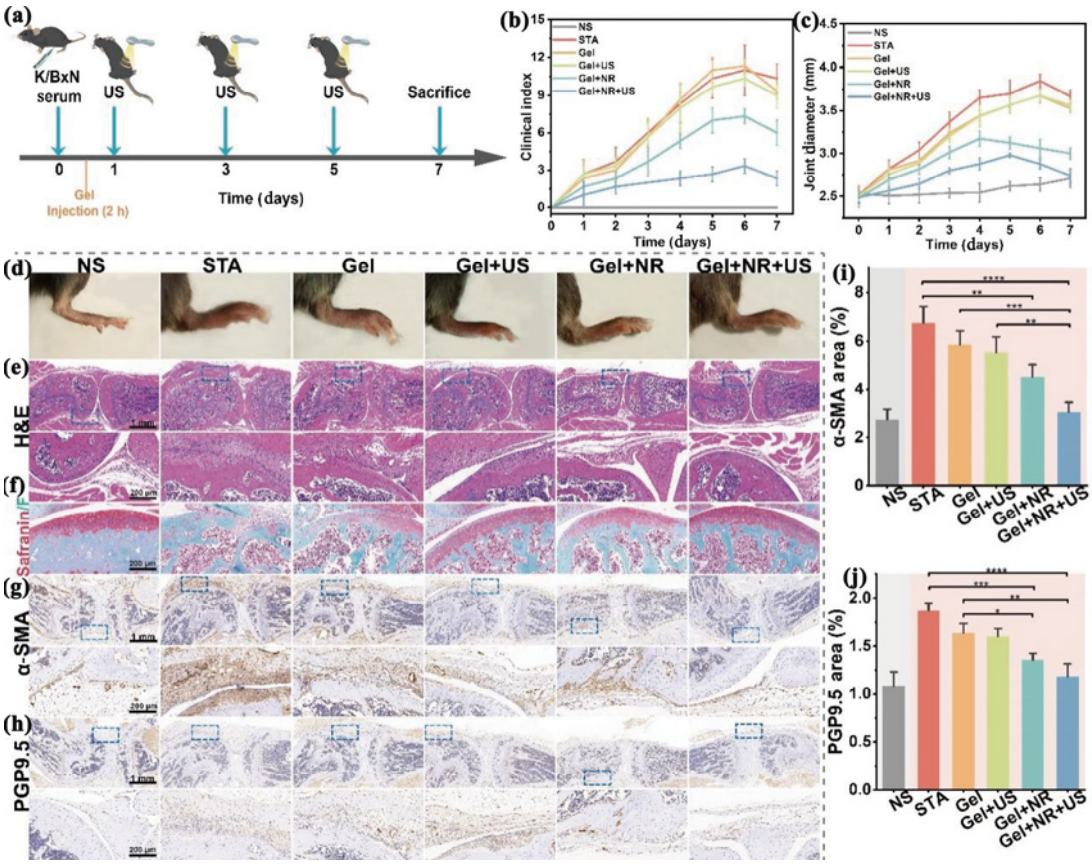

Fig. 3 USNR eliminating RA symptoms and pathologies. (a) Animal experiment timeline. (b, c) Clinical indexes and joint diameters, respectively. (d) Photos of mice claws. (e–h) H&E, safranin/F, and immunohistochemistry (α-SMA and PGP9.5) of knee joint. (i, j) α-SMA and PGP9.5 area percentages in synovium, respectively. All data are presented as mean±standard deviation (SD), number of experiment (n) = 3. Statistical analysis of data conforming to normal distribution was carried out using one-way analysis of variance (ANOVA), followed by Tukey post hoc test (equal variances).

signal can slightly alleviate RA. Under US stimulation, the piezoelectric signal produced by NR can be more effectively used in the treatment of RA. The hematoxylin eosin (H&E) results show that synovium of STA model thickens, a large number of immune cells infiltrate, and bone cartilage erodes (Fig. 3(e)). After NR applied, the situation had slightly improved, while Gel+NR+US significantly inhibited synovial thickening and immune cell infiltration, making it close to NS group. The safranin/F results show that the joints of STA model are barely stained with safranin, indicating that articular cartilage is damaged, and the polysaccharide protein in cartilage is reduced (Fig. 3(f)). After Gel+NR+US treatment, the cartilage is significantly stained compared with other treatment groups, approaching NS group, indicating its effect of inhibiting the erosion of RA cartilage.

When RA occurs, the vascular density increases, which provides conditions for inflammatory cell infiltration, and forms pannus together with macrophages, fibroblasts, etc., thereby eroding osteochondral [1]. Therefore, the decrease of synovial vascular density is an important evaluation index for the remission of RA. The immunohistochemical results of α-SMA, a vascular marker, show that the vascular density at the synovium of STA model increased significantly; and after Gel+NR+US treatment, compared with those of the other treatment groups, the vascular density decreases significantly, approaching the NS level (Figs. 3(g) and 3(i)). References [26,27] showed that the increased angiogenesis in RA is accompanied by the increased nerve ingrowth, which leads to increased pain in RA patients. Interestingly, our study shows that STA model does increase the expression of PGP9.5, a neural marker, while Gel+NR+US treatment significantly does reduce the expression of PGP9.5 (Figs. 3(h) and 3(j)). Therefore, USNR does reverse the HVN, thus inhibiting the progress of synovitis and conducing the cure of RA.

4 USNR reprograming macrophages in RA

Macrophages are important participants in the progress and remission of RA [28]. The classical theory divides macrophages into M1 (pro-inflammatory phenotype) and M2 (pro-healing phenotype) [1]. The ratio of M1 and M2 changes dynamically during the occurrence and remission of inflammation. Acute RA inflammatory phase is characterized by a dominated percentage of pro-inflammatory M1 phenotype [3]. They interact and influence with other types of cells in synovitis progression and bone erosion, including FLSs and cells of innate and adaptive immune systems [14]. It is considered to be an effective therapy for RA to induce the reprogramming of macrophages from the proinflammatory phenotype to the anti-inflammatory phenotype [29]. On the other hand, Refs. [7–11] have reported that appropriate piezoelectric stimulation can reprogram macrophages including inducing anti-inflammatory phenotype, which may help to patch this barrier. Herein, we try to explore the effect of USNR on macrophage reprogramming in RA. The immunohistochemistry and immunofluorescence results show that STA significantly increases the infiltration of macrophages, while Gel+NR+US treatment significantly reduces the infiltration of macrophages compared with any other treatment groups (Figs. 4(a)–4(d)). Therefore, USNR may alleviate inflammation by reducing total macrophage infiltration. Therefore, we perform immunofluorescence labeling imaging on M1 and M2 at day 7. The results show that in STA, Gel, and Gel+US treatment group, M1 is dominant, indicating that it is in the stage of inflammation, and US itself cannot drive macrophage toward M2 polarization in the STA condition (Fig. 4(c)). Intriguingly, in the Gel+NR group, some macrophages are polarized to the M2 phenotype, which can be attributed to the piezoelectric effect induced by physiological movement of mice [30]. While in Gel+NR+US group, the macrophage phenotype is reversed, M2 phenotype dominating (Fig. 4(d)). In order to further verify that USNR can regulate the phenotype of macrophages, RAW264.7 is 3D cultured. With or without lipopolysaccharides (LPS) induction, USNRs inhibit the expression of pro-inflammatory genes and promote the expression of pro-healing genes (Figs. 4(i) and 4(j)).

Recently, FAP-α^+ FLS is found in RA synovium and plays a “key” role in the progression of RA disease [31]. Clearing FAP-α^+ FLS is considered to be a potential RA therapy, but there is no report on clearing FAP-α^+ FLS to treat RA at present. Here, the distribution of FAP-α in mouse synovium is studied. The results show that STA, Gel, and Gel+US groups have high levels of FAP-α expression, Gel+NR treatment group slightly reduces FAP-α expression, while Gel+ NR+US significantly reduces FAP-α expression compared with any other groups (Figs. 4(f)

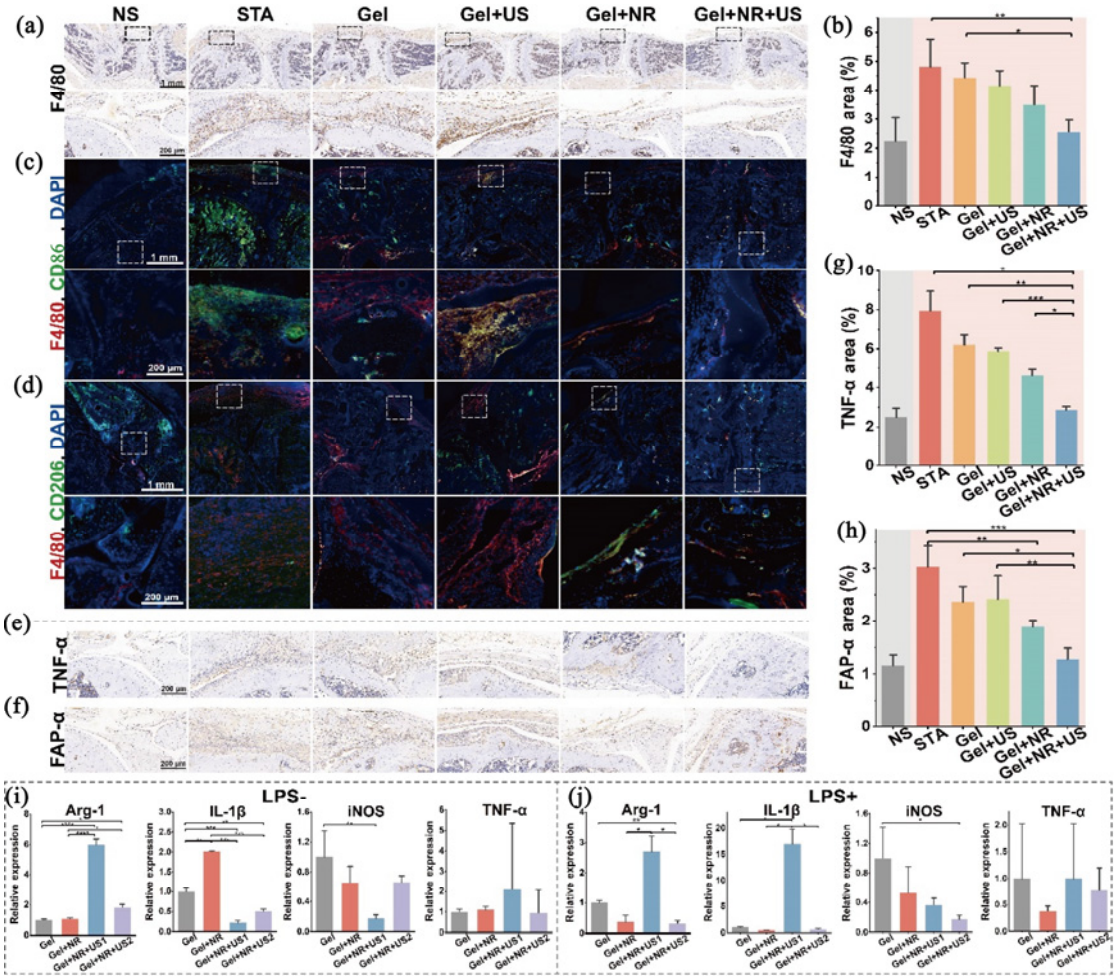

Fig. 4 USNR reprograming macrophages in RA. (a) Immunohistochemistry (F4/80) of knee joint. (b) F4/80 area percentages in synovium. (c, d) Immunofluorescence (F4/80, CD86, 4′,6-diamidino-2-phenylindole (DAPI) and F4/80, CD206, DAPI, respectively) of knee joint. (e, f) Immunohistochemistry (TNF-α and FAP-α, respectively) of synovium of knee joint. (g, h) TNF-α and FAP-α area percentages in synovium, respectively. (i, j) Quantitative real time-polymerase chain reaction (qRT-PCR) results of RAW264.7 in LPS− and LPS+ conditions, respectively. All data are presented as mean±SD, $n = 3$. Statistical analysis of data conforming to normal distribution uses one-way ANOVA, followed by Tukey post hoc test (equal variances) and by Games–Howell post hoc test (unequal variances). Comparisons between groups of data that do not conform to a normal distribution use Kruskal–Wallis nonparametric test.

and 4(h) and Fig. S8 in the ESM). Therefore, USNR can significantly clear FAP-α^+ FLS, which may be attributed to the macrophage polarization from M1 to M2. In RA, inflammatory factors are mainly secreted by M1 macrophages and pro-inflammatory FLS. TNF-α is a key inflammatory factor in RA [32]. Antagonists targeting TNF-α have been developed clinically and have achieved good curative effects in the treatment of RA [32]. It is demonstrated that the US applied on empty gel slightly alleviates the inflammation, but it shows no significant effect, while Gel+NR+US significantly reduces TNF-α and brings nearly back to the healthy level (Figs. 4(e) and 4(g) and Fig. S8 in the ESM), further confirming the electric-stimulation effects of USNR. The reduction of TNF-α can be also attributed to the transformation of macrophages from M1 type to M2 type and the reduction of FAP-α^+ FLS.

5 USNR patching immunologic barrier

To explore the reprogramming effect of USNR on TREM2$^+$ TRM, Cx3cr1creRosa26 (R26)-tdTomato genotype mice is used to induce the specific expression of tdTomato fluorescent protein in TREM2$^+$ TRM by injecting tamoxifen due to that these barrier macrophages specifically express Cx3cr1 [5]. It is verified in NS

mice that the barrier macrophages of this genotype mice do express tdTomato fluorescent protein, and this layer of macrophages is closely connected (Fig. 5(a)), providing physical and immunologic barrier protection for the articular cavity. After STA model induction, the orientation of $TREM2^+$ TRM changes, and the immunologic barrier is disrupted. After Gel+NR+US treatment, $TREM2^+$ TRM reconnects again, and the barrier is restored (Fig. 5(b)), which may due to that negative charge generated by USNR affects the binding of the TREM2 receptor to the ligand, thus altering the activation of the downstream pathway based on Ref. [13]. These results indicate that USNR could effectively patch this layer of macrophage barrier, thereby keeping joint immune homeostasis.

6 TREM2 playing an indispensable role in curing RA mediated by USNR

TREM2 was reported to play an important role in other pathological processes such as Alzheimer's disease, where inhibiting hydrolysis and abscission of TREM2 can promote macrophage phagocytosis, increase macrophage survival, and inhibit inflammation [14–21]. However, the role of TREM2 in RA has not been reported so far. More importantly, TREM2 prefers to bind with negatively charged ligand [15]. This inspired us of the idea that the behaviors of $TREM2^+$ TRM may be influenced by the change of the intrinsic binding between TREM2 with negatively charged ligand via the charges generated by USNR. TREM2 KO genotype mice are used for validation. Herein, the negative effect of TREM2 deficiency in the experimental animal model of RA is reported for the first time. It is demonstrated in this work that TREM2 deficiency aggravates RA symptoms (Figs. 6(a), 6(b), 6(f), 6(h), 6(p), and 6(r)) and pathologies (Figs. 6(c)–6(e), 6(j), 6(l), and 6(n)) in STA mice model, and inflammation in TREM2 deficiency STA mice is more severe compared with that in normal STA mice (Figs. 6(d), 6(e), 6(l), and 6(n)). On the other hand, compared with the results of Gel+NR+US treatment on TREM2 deficiency and normal mice, it demonstrated that the clinical score and swelling degree of TREM2 deficiency mice is higher than that of normal mice (Figs. 6(q) and 6(s)). Moreover, further study demonstrates that macrophage infiltration (Figs. 6(c) and 6(k)), FAP-α^+ FLS (Figs. 6(e) and 6(o)), and tumor necrosis factor TNF-α (Figs. 6(d) and 6(m)) levels are statistically higher in the Gel+NR+US treated TREM2 KO mice. Therefore, the TREM2 deficiency compromises the therapeutic effect in Gel+NR+US group, which suggests that TREM2 is an important receptor mediating the treatment of RA by USNR. What is more, even in the case of TREM2 KO, USNR resulted in a slight relief of arthritis symptoms (Fig. S9 in the ESM). These results together reveal that TREM2 may become a potential new target of RA, and TREM2 does play an indispensable role in curing RA mediated by USNR.

7 Conclusions

We prepare piezoelectric tetragonal BTO USNR by the solvothermal synthesis method, which can generate controllable electrical stimulation in response to ultrasound to cure RA by minimally invasive injection into joint cavity. USNR can eliminate RA symptoms including joint swelling degree and joint score, and RA pathologies including osteochondral erosion, inflammatory infiltration, and HVN. USNR can reprogram macrophages, including inducing macrophages in RA to change from an inflammatory phenotype to an anti-inflammatory

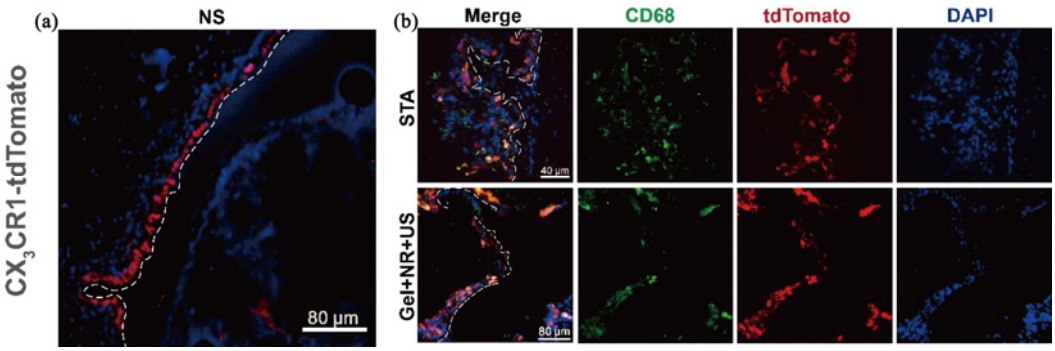

Fig. 5 USNR patching immunologic barrier. Fluorescence imaging of macrophage barrier by Cx3cr1creR26-tdTomato genotype mice in (a) NS and (b) STA and Gel+NR+US.

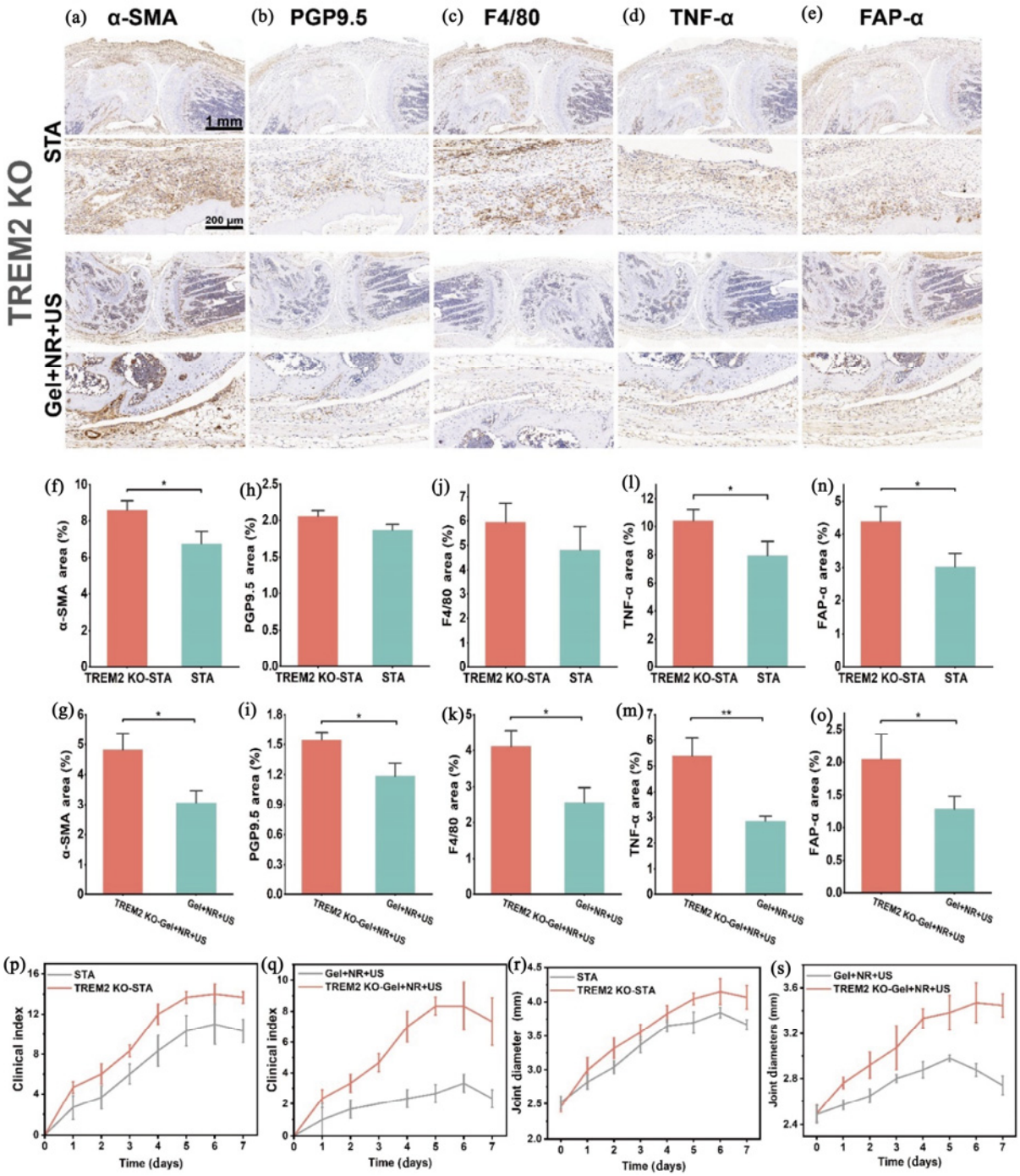

Fig. 6 TREM2 playing an indispensable role in curing RA mediated by USNR. Immunohistochemistry of knee joint in TREM2 KO mice for (a) α-SMA, (b) PGP9.5, (c) F4/80, (d) TNF-α, and (e) FAP-α. Comparison of TREM2 KO mice and normal mice by the quantification of immunohistochemistry positive area percentages of (f, g) α-SMA, (h, i) PGP9.5, (j, k) F4/80, (l, m) TNF-α, and (n, o) FAP-α for both STA and USNR treatments. (p–s) Joint diameters and clinical indexes of TREM2 KO mice and normal mice under conditions of STA and USNR treatment. All data are presented as mean±SD, n = 3. Statistical analysis of data conforming to normal distribution was carried out using one-way ANOVA, followed by Tukey post hoc test (equal variances).

phenotype, and patching TREM2$^+$ TRM immunological barrier. Further research discovers that TREM2 does play an indispensable role in curing RA mediated by USNR. In all, a deliberate strategy for patching the immunologic barrier by a novel USNR is reported in our work for the first time, which initiates a paradigm for curing RA by controlling the potential drivers via advanced ceramics.

8 Materials and methods

8. 1 Synthesis of tetragonal BTO

BTO nanoparticles were prepared by the solvothermal process of $Ba(OH)_2{\cdot}H_2O$ (98%, Macklin) and $Ti[O(CH_2)_3CH_3]_4$ (97%, Sigma-Aldrich). During the synthesis, 3.4036 g (10 mmol) of $Ti[O(CH_2)_3CH_3]_4$ was dissolved in 4 mL of high-purity ethanol, and then mixed with 1.4 mL of NH_4OH solution (28%–30% NH_3 in H_2O, Sigma-Aldrich) under vigorous stirring. Following this, 2.8408 g (15 mmol) of $Ba(OH)_2{\cdot}H_2O$ (barium/titanium ratio = 1.5) was dissolved in 5 mL of deionized water and added to the above solution. The final solution was transferred to a 50 mL Teflon-lined stainless steel autoclave and heated preservation at 200 ℃ for 48 h. The resulting product was thoroughly washed with acetic acid, high-purity ethanol, and water, and then dried at 80 ℃. The product was heated in the oven for 2 h, and acetic acid was used to remove BaO or $BaCO_3$ or both from the product.

8. 2 Synthesis of injectable piezoelectric NR hydrogel

Rat tail-derived collagen I (Corning Ltd., Beijing) was used to obtain an injectable piezoelectric hydrogel according to the manufacture's protocol. In short, the collagen I solution dissolved in acetic acid was neutralized with NaOH, and then added NR to disperse evenly and put at 37 ℃ for 20 min to form a piezoelectric hydrogel.

8. 3 Characterization of piezoelectric NR hydrogel

The SEM photographs were obtained by a field-emission high-resolution SEM (Zeiss; 15 kV). The TEM photographs were recorded by a field-emission TEM (JEM-2100F, JEOL; 200 kV). The XRD patterns were measured on an X-ray diffractometer (D/max-2550, Rigaku; parameters: Cu Kα, λ = 1.54 Å, 40 mA, and 40 kV). The hydrated particle sizes were obtained by Malvern nanosize. The XPS spectra were conducted on an X-ray spectrometer (Escalab 250Xi, Thermal Scientific). The Raman spectra were recorded by the Raman spectrometer (LabRAM HR Evolution, Horiba).

8. 4 3D culture of RAW264.7 and US treatment

100 μg/mL BTO and 5×10^5 cells/mL RAW264.7 were evenly dispersed into 2 mg/mL collagen solution. Subsequently, the collagen hydrogel was fully gelatinized by incubating in a humified incubator for 30 min, and macrophages were 3D cultured in the hydrogel. Then the medium containing 10% fetal bovine serum (FBS) and 1% penicillin–streptomycin was added in a humidified incubator. All experiments involving US treatment were conducted using a US transducer (Chattanooga Co.). The surface of US transducer was evenly coated with medical ultrasonic gel, which was in direct contact with the bottom of cell culture orifice plate.

The US1 is an ultrasound wave with a frequency of 1 MHz, power of 1.2 W/cm^2, and duty ratio of 50%, performing 3 min; the US2 is an ultrasound wave with a frequency of 3 MHz, power of 1.0 W/cm^2, and duty ratio of 50%, performing 3 min. Considered the better anti-inflammatory effect of US1, it was chosen to further perform the *in vivo* experiments.

8. 5 qRT-PCR

SD-bone marrow mesenchymal stem cells (BMSCs) were cultured in osteogenic differentiation Kit (RAXMX-90021, Oricell). RAW264.7 was cultured in Dulbecco's modified eagle medium (DMEM) supplemented with 10% FBS, 1% penicillin (50 U/mL), and streptomycin (50 U/mL) (Procell Life Science & Technology Co., Ltd.) in a 5% CO_2 atmosphere at 37 ℃ for 24 h. The medium was replaced by 2 μg/mL LPS for 12 h, and then incubated in the culture medium for another 24 h. To exam the mRNA of targeted genes in SD-BMSCs and RAW264.7, the qRT-PCR was performed firstly, extracting the total RNA by the micro RNA (miRNA) isolation Kit (miRcute, Tiangen Biotech (Beijing) Co. Ltd.) according to the manufacturer's protocol; secondly, complementary DNA (cDNA) from the RNA extracted using the RT kit (FastQuant, Tiangen Biotech (Beijing) Co. Ltd., China) was acquired; and finally, the qRT-PCR on real-time PCR (CFX96, Bio-Rad) using iTaq Universal SYBR Green Supermix (172-5122, Bio-Rad) was performed, where glyceraldehyde-3-phosphate dehydrogenase (GAPDH) was used as the internal control, and the sequence of primers is listed in Table S1 in the ESM.

8. 6 Mice

Cx3cr1creR26-tdTomato genotype mice were purchased from Shanghai Southern Model Biology Company. The expression of tdTomato fluorescence was induced by the injection of tamoxifen. KRN mice were presented by Prof. Christophe Benoist and Prof. Diane Mathis of Harvard Medical School. After mating with NOD/LtJ mice, K/BxN mice with spontaneous

arthritis were obtained. The above animals were raised in the barrier of the Experimental Animal Center of Tsinghua University, and the experimental animal program was approved by the Institutional Animal Care and Use Committee (IACUC) of Tsinghua University (with the AP number: 21-SXD3). All mice were genotyped by PCR before use.

8. 7 *In vivo* experiments and arthritis induction

K/BxN STA was induced by injecting K/BxN serum collected from arthritis K/BxN mice. The clinical development of arthritis was assessed using a clinical index of 0 (minimum)–16 (maximum), which indicates that the cumulative score of each claw is 0–4: 0 = no signs of inflammation, 1 = slightly swollen and red claws or only affect a single finger, 2 = moderate swelling and erythema or multiple fingers affecting each claw, 3 = severe swelling and erythema affecting the whole claw, and 4 = maximum swelling and erythema. A vernier caliper was used to measure the swelling of the hind-paw.

Cx3cr1creR26-tdTomato genotype mice were treated twice intraperitoneally (i.p.) with 4 mg of tamoxifen dissolved in peanut oil within 48 h. K/BxN serum metastatic arthritis was induced 5 d after injection. Mice were sacrificed 7 d after induction of arthritis. 40 μL blank hydrogel or piezoelectric hydrogel was injected into intraarticular of mice, and the concentration of BTO in piezoelectric hydrogel is 100 mg/kg. The mice in the US treatment group were irradiated with US1 (1.0 MHz, 1.2 W/cm^2, 50% duty cycle, and 3 min) at 3 h, 1 d, and 3 d after injection.

8. 8 Paraffin section of mouse knee joint

Mouse long bones containing knee joints were fixed in 4% paraformaldehyde (PFA)/phosphate buffered saline (PBS) (pH = 7.4) for 12 h, and then incubated in demineralized solution for one month. Tissue samples were dehydrated to transparency by a series of graded ethanol, and then embedded in paraffin. Paraffin sections were stained with H&E to detect knee inflammation and Saffron O–fast green staining to detect cartilage damage. During immunohistochemical staining, the sections were incubated with primary antibodies overnight at 4 ℃, washed three times with phosphate buffered saline with Tween (20 PBST), and incubated with secondary antibodies (Beyotime Institute of Biotechnology) at room temperature for 2 h.

8. 9 Frozen section of mouse knee joint

Mouse long bones containing knee joints were fixed in 4% PFA/PBS (pH = 7.4), fixed at 4 ℃ for 12 h, cultured in decalcification buffer (14% ethylene diamine tetraacetic acid (EDTA), NH_4OH, pH = 7.2) for 10 d, and embedded with optimal cutting temperature (OCT) compound (Sakura Finetek). The freezing microtome (cm1900, Leica) and frozen tape were used to make 7 μm thick tissue sections.

8. 10 Histological immunofluorescence staining and imaging

In order to stain the frozen sections of mouse knee joints, the samples were blocked with 10% goat serum and permeated with 0.3% Triton at room temperature for 1 h. The antibodies used here are listed as follows: CD68 (sc-20060 AF488, Santa), F4/80 (GB113373, Servicebio), TREM2 (DF12529, Affinity), FAP-α (AF0739, Affinity), CD206 (sc-70585, Santa), CD86(105001, Biolegend), α-SMA (67735-1-Ig, Proteintech), and PGP9.5 (14730-1-AP, Proteintech). The primary antibody with blocking solution was diluted and incubated overnight at 4 ℃. The unbound primary antibody was washed with Dulbecco's phosphate buffered saline (DPBS), and the unlabeled primary antibody was counterstained with Goat anti-rabbit IgG AF649 (P03S17, Gplink) or Goat anti-mouse AF488 antibody (P03S18S, CST) in closed solution at room temperature for 4 h, and washed with DPBS. The DAPI sealing agent (ab104139, Abcam) was used to insert the cover glass. The histological immunofluorescence imaging was conducted by the spinning disk confocal microscopy (Dragonfly, Andor) and automatic digital slide scanning system (Axio Scan. Z1, Zeiss). The quantification of the immunohistochemistry imaging was handled by Image J software.

8. 11 Statistical analysis

Unless otherwise stated, data were expressed as mean±SD. All quantitative experiments were performed at least three times. SPSS software (v.23.0, IBM Corp.) was used for normality test, homogeneity of variance test, and significant difference analysis. The comparison of the two groups of data in this paper was in line with the normal distribution, and the corresponding significant difference was analyzed by the Independent Samples t-test. Comparisons among multiple groups of normally distributed data were performed using one-way ANOVA

followed by Tukey post hoc test (equal variances) or Games–Howell post hoc test (unequal variances). Comparisons between groups of data that do not conform to a normal distribution were performed using Kruskal–Wallis nonparametric tests.

Acknowledgements

The authors would like to acknowledge the assistance of Yanli Zhang, Imaging Core Facility, Technology Center for Protein Sciences, Tsinghua University, for the assistance of using the spinning disk confocal microscopy (Dragonfly, Andor); Yue Sun, Center of Biomedical Analysis, Tsinghua University, for the assistance of using the automatic digital slide scanning system (Axio Scan. Z1, Zeiss); Jingjing Wang, Center of Biomedical Analysis, Tsinghua University, for the assistance of using the microscopy slide scanner (Pannoramic SCAN, 3D HISTECH); Prof. Christophe Benoist, Harvard University, for his generous donation of KRN mice; and Prof. Xin Lin, Department of Immunology, Tsinghua University, for his generous donation of TREM2 KO mice.

Fundings

This work was supported by the National Natural Science Foundation of China (Grant Nos. 52072210 and 52111530230), Key R&D Projects of Social Development of Hainan Provincial Department of Science and Technology (Grant No. ZDYF2020137), and Tsinghua University Beijing Union Medical College Hospital Cooperation Project (Grant No. 20191080871).

Declaration of competing interest

The authors have no competing interests to declare that are relevant to the content of this article.

Electronic Supplementary Material

Supplementary material is available in the online version of this article at https://doi.org/10.26599/JAC.2023.9220730.

References

[1] Zhang F, Wei K, Slowikowski K, *et al*. Defining inflammatory cell states in rheumatoid arthritis joint synovial tissues by integrating single-cell transcriptomics and mass cytometry. *Nat Immunol* 2019, **20**: 928–942.

[2] Schett G, Tanaka Y, Isaacs JD. Why remission is not enough: Underlying disease mechanisms in RA that prevent cure. *Nat Rev Rheumatol* 2021, **17**: 135–144.

[3] Gang FL, Zhang Q, Jiang L, *et al*. Thermochemotherapy meets tissue engineering for rheumatoid arthritis treatment. *Adv Funct Mater* 2021, **31**: 2104131.

[4] McInnes IB, Schett G. Pathogenetic insights from the treatment of rheumatoid arthritis. *Lancet* 2017, **389**: 2328–2337.

[5] Culemann S, Grüneboom A, Nicolás-Ávila JÁ, *et al*. Locally renewing resident synovial macrophages provide a protective barrier for the joint. *Nature* 2019, **572**: 670–675.

[6] Alivernini S, MacDonald L, Elmesmari A, *et al*. Distinct synovial tissue macrophage subsets regulate inflammation and remission in rheumatoid arthritis. *Nat Med* 2020, **26**: 1295–1306.

[7] Dai XH, Heng BC, Bai YY, *et al*. Restoration of electrical microenvironment enhances bone regeneration under diabetic conditions by modulating macrophage polarization. *Bioact Mater* 2021, **6**: 2029–2038.

[8] Wang ZY, He XZ, Tang BL, *et al*. Polarization behavior of bone marrow-derived macrophages on charged P(VDF–TrFE) coatings. *Biomater Sci* 2021, **9**: 874–881.

[9] Hoare JI, Rajnicek AM, McCaig CD, *et al*. Electric fields are novel determinants of human macrophage functions. *J Leukoc Biol* 2016, **99**: 1141–1151.

[10] Li CM, Levin M, Kaplan DL. Bioelectric modulation of macrophage polarization. *Sci Rep* 2016, **6**: 21044.

[11] McLean NA, Verge VMK. Dynamic impact of brief electrical nerve stimulation on the neural immune axis—Polarization of macrophages toward a pro-repair phenotype in demyelinated peripheral nerve. *Glia* 2016, **64**: 1546–1561.

[12] Zhu P, Chen Y, Shi JL. Piezocatalytic tumor therapy by ultrasound-triggered and $BaTiO_3$-mediated piezoelectricity. *Adv Mater* 2020, **32**: 2001976.

[13] Zhao D, Feng PJ, Liu JH, *et al*. Electromagnetized-nanoparticle-modulated neural plasticity and recovery of degenerative dopaminergic neurons in the mid-brain. *Adv Mater* 2020, **32**: 2003800.

[14] Zagórska A, Través PG, Lew ED, *et al*. Diversification of TAM receptor tyrosine kinase function. *Nat Immunol* 2014, **15**: 920–928.

[15] Deczkowska A, Weiner A, Amit I. The physiology, pathology, and potential therapeutic applications of the TREM2 signaling pathway. *Cell* 2020, **181**: 1207–1217.

[16] Katzenelenbogen Y, Sheban FD, Yalin A, *et al*. Coupled scRNA-seq and intracellular protein activity reveal an immunosuppressive role of TREM2 in cancer. *Cell* 2020, **182**: 872–885.e19.

[17] Molgora M, Esaulova E, Vermi W, *et al*. TREM2 modulation remodels the tumor myeloid landscape enhancing anti-PD-1 immunotherapy. *Cell* 2020, **182**: 886–900.e17.

[18] Wang YM, Cella M, Mallinson K, *et al*. TREM2 lipid sensing sustains the microglial response in an Alzheimer's

disease model. *Cell* 2015, **160**: 1061–1071.
[19] Ulland TK, Song WM, Huang SCC, *et al*. TREM2 maintains microglial metabolic fitness in Alzheimer's disease. *Cell* 2017, **170**: 649–663.e13.
[20] Schlepckow K, Monroe KM, Kleinberger G, *et al*. Enhancing protective microglial activities with a dual function TREM2 antibody to the stalk region. *EMBO Mol Med* 2020, **12**: e11227.
[21] Ewers M, Franzmeier N, Suárez-Calvet M, *et al*. Increased soluble TREM2 in cerebrospinal fluid is associated with reduced cognitive and clinical decline in Alzheimer's disease. *Sci Transl Med* 2019, **11**: eaav6221.
[22] Lee HW, Moon S, Choi CH, *et al*. Synthesis and size control of tetragonal barium titanate nanopowders by facile solvothermal method. *J Am Ceram Soc* 2012, **95**: 2429–2434.
[23] Wu J, Xu Q, Lin EZ, *et al*. Insights into the role of ferroelectric polarization in piezocatalysis of nanocrystalline $BaTiO_3$. *ACS Appl Mater Interfaces* 2018, **10**: 17842–17849.
[24] Adireddy S, Lin CK, Cao BB, *et al*. Solution-based growth of monodisperse cube-like $BaTiO_3$ colloidal nanocrystals. *Chem Mater* 2010, **22**: 1946–1948.
[25] DiDomenico M, Wemple SH, Porto SPS, *et al*. Raman spectrum of single-domain $BaTiO_3$. *Phys Rev* 1968, **174**: 522–530.
[26] Mapp PI, Walsh DA. Mechanisms and targets of angiogenesis and nerve growth in osteoarthritis. *Nat Rev Rheumatol* 2012, **8**: 390–398.
[27] Delay L, Barbier J, Aissouni Y, *et al*. Tyrosine kinase type A—Specific signalling pathways are critical for mechanical allodynia development and bone alterations in a mouse model of rheumatoid arthritis. *Pain* 2022, **163**: e837–e849.
[28] Udalova IA, Mantovani A, Feldmann M. Macrophage heterogeneity in the context of rheumatoid arthritis. *Nat Rev Rheumatol* 2016, **12**: 472–485.
[29] Boutet MA, Courties G, Nerviani A, *et al*. Novel insights into macrophage diversity in rheumatoid arthritis synovium. *Autoimmun Rev* 2021, **20**: 102758.
[30] Liu Y, Dzidotor G, Le TT, *et al*. Exercise-induced piezoelectric stimulation for cartilage regeneration in rabbits. *Sci Transl Med* 2022, **14**: eabi7282.
[31] Croft AP, Campos J, Jansen K, *et al*. Distinct fibroblast subsets drive inflammation and damage in arthritis. *Nature* 2019, **570**: 246–251.
[32] Marotte H, Miossec P. Prevention of bone mineral density loss in patients with rheumatoid arthritis treated with anti-TNFα therapy. *Biologics* 2008, **2**: 663–669.